ITT INDUSTRIAL LABORATORIES
FORT WAYNE, INDIANA

APPLICATIONS NOTE

NO. E6

UNIQUE PROPERTIES

OF

IMAGE DISSECTORS

12/3/63

A DIVISION OF INTERNATIONAL TELEPHONE AND TELEGRAPH CORPORATION

The term "image dissector" or more concisely "dissector" is applied by ITTIL to a scanned pickup tube. In this tube an input radiant energy image is focused onto a photocathode, followed by an electron optical focusing system forming an electron image of the emitted photoelectrons in the plane of a small defining aperture. An electron multiplier follows this aperture, and a deflection system, either magnetic or electric, is included for deflecting the electron image over the defining aperture in such a way that various portions of the image are examined in sequence.

The dissector as thus defined has unique and rather unusual properties not generally recognized which should be taken into consideration when selecting an appropriate camera tube for a specific application:

1. Non-Storage

Because no storage is involved, the scan rate on a dissector can be varied at will without changing the signal current amplitude. In fact the scan can be stopped completely at any image point or points at which further detailed information is desired. Dual or multiple scan modes can also be adopted, in which an earlier large raster scan is replaced by a smaller scanned area for image analysis or image tracking. This ability to vary the scan speed and raster size is quite unique with the image dissector and is so unusual that it is often overlooked in new design considerations.

2. Panned-Camera

Directly related to nonstorage operation is the ability of the dissector to operate with a panned or nonstabilized platform. Since no information storage, over a preceding comparatively long frame time or line time is required, the camera platform need not be stabilized for that same period. Full resolving power is retained in the dissector if the platform remains stable within one resolution element only for the "dwell-time" on each resolution element, rather than for the total frame time. This is a relaxation of the platform stabilization requirements by a factor equal to the total number of resolvable picture elements. Image distortion resulting from panning can, of course, be removed during data processing.

3. High Resolution

Image dissectors achieve paraxial resolutions closely predictable on the basis of selected electron beam defining aperture size. For example, in magnetically focused tubes, contrast ratios as high as 40 percent have been observed experimentally with 0.001 inch diameter apertures at 1600 TV lines/inch resolving power (800 line pairs/inch). These high resolutions are quite compatible with the ultimate limits set by the emission energies of the photoelectrons for tubes of this type, as established by G. Papp of ITTIL (IRE Tr. on Nuclear Science, Vol NS-9, No. 2, April 1962, p 93).

Off-axis resolution approaching the paraxial performance can be achieved with a moderate degree of dynamic focusing only in magnetically-focused varieties. For electrostatically focused dissectors, off-axis loss of resolution, even with dynamic focusing is appreciable.

4. Linearity

The basic multiplier phototube operating principle used in image dissectors is linear over many orders of magnitude, at least 4 to 5 orders in normal usage. The image dissector is therefore particularly useful where a wide dynamic range of signal inputs with linear response is encountered. Even greater dynamic range can be accommodated by re-adjustment of the multiplier gain by altering the applied operating potentials.

Response linearity from one portion of an input image to another portion of the same image is limited to some extent, as it would be in any camera tube, by internal light reflections within the camera tube envelope. Dissectors with internal optical trapping can be supplied on special order.

5. Noise

Noise in an image dissector camera normally arises from three readily identified sources: dark emission from the photocathode, background lighting on the photocathode, and the signal flux itself. The multiplier gain is normally high enough so that other noise sources, such as amplifier noise etc. are negligible. With nearly all photocathodes except infrared sensitive types the dark emission noise is also negligible, so that the dissectors, in general, operate either under a background noise limited or a noise-in-signal limited condition. Photon fluctuations of the flux input, modified by the quantum efficiency of the photoemissive conversion process at the photocathode, are then observable in the dissector. For location of images on a dark background, as in star tracking, the dissector may therefore be more sensitive than expected because of the almost total absence of dark noise in the nonsignal areas.

See ITTIL Research Memo 386 for additional information on dissector noise.

6. Special Apertures

Dissectors are readily adapted to the examination of specialized portions of the input image using appropriately shaped defining apertures. Apertures can range from a long slit aperture for examining single line scans of a spectrum to such complex apertures as pin-wheels, etc., used with special scan modes to obtain additional picture information or discriminate against certain input patterns.

7. Multiple Apertures

By appropriate electron optical techniques, two or more separate electron multipliers can be placed behind appropriate dissector apertures to achieve simultaneous differential readout of picture information. This can be useful in character recognition and other specialized problem areas.

8. Simple Operating Theory

The operational theory of the dissector is simple and straightforward, making it possible to predict, a priori, what the resulting system capabilities will be. This is useful to the system designer and in the system check-out. See, for example, "Reference Data for Radio Engineers" ITT Corporation, 4th Edition, p 410.

9. Reliability

The dissector is a simple, rugged, reliable device without a thermionic cathode, which limits the lifetime and consumes operating power. Shelf life is many years and operating life is comparable, unless excessive input illumination occurs for long time periods. Momentary exposure to sunlight or even the sun's image does no harm. No delicate films or vibration sensitive parts are required.

10. Fast Turn On

The dissector is ready to operate at full efficiency as fast as the associated circuitry can be activated.

11. Scan Drive

The dissector is adaptable to both magnetic and electric deflection, although magnetic deflection has proven to be more readily adaptable to low power transistor drive circuitry. If fast fly back or fast random access is not required, a dissector with magnetic scan can supply large amounts of picture information at high output signal levels, with a minimum of total required system power.

12. Spectral Response

This extends over all regions for which suitable photocathodes are available and therefore includes the near infrared to the extreme ultraviolet region. Windowless dissectors capable of operating into the X-ray region can be constructed.

13. Raster Edge Effects

Unlike such beam scanning tubes as the image orthicon and vidicon, the dissector has no scanned raster area surrounded by an uncharged unscanned area. As a result no edge effects are encountered in the dissector resulting from potential discontinuities at the raster edge and showing up as abnormal signal amplitudes along all raster edges as observed in image orthicons and vidicons. A small raster, of for example only 5 or 6 short scan lines can be located anywhere on the dissector sensitive area, with each scan line, even at the edges, contributing proper signal amplitudes, and with no raster "burn-in".

14. Size

Dissectors can be constructed in a wide variety of sizes to meet specialized requirements. There are no restrictions on thin film size (as in the image orthicon), gun size, etc., 1 inch, 1-1/2 inch, and 4-1/2 inch O.D. sizes are presently available from ITTIL, and 1/2 inch, 3/4 inch, and 2 inch sizes, as well as larger varieties are available on special order. The 1 inch and 1-1/2 inch sizes are designed to operate with standard vidicon coil systems.

ITTIL has prepared a number of Research Memos and other publications concerning image dissectors available on request. These include Research Memos Nos. 309, 336, 353, and 386, as well as applications notes on the FW-146/FW-125 image dissectors. ITTIL has been a pioneer in the development of image dissectors since the earliest days of television, when Philo T. Farnsworth of ITTIL developed the image dissector as the earliest all-electronic television scanning pickup device.

ITTIL will be pleased to cooperate with prospective customers requesting more information regarding image dissector principles and the latest developmental advancements, or requiring special tube design to meet individual system specifications. Please contact Component Sales, ITT Industrial Laboratories, 3702 E. Pontiac Street, Fort Wayne, Indiana.

ITT Industrial Laboratories, Ft. Wayne, Indiana

RESEARCH MEMO 401

DAYTIME STAR ACQUISITION AND TRACKING USING THE IMAGE DISSECTOR

E. H. Eberhardt
May 14, 1964

1.0 INTRODUCTION

This memo discusses the problem of locating and tracking a star within a certain optical field of view in daylight using an image dissector. The basic problem is to be able to identify the precise location of the star in the presence of an obscuring sky brightness background signal.

This memo is concerned only with the problem of daytime operation. At night or in space, the image dissector, because of its low dark noise, as pointed out by Salinger (Ref. 4) and Laverty (Ref. 5) becomes the method of choice.

2.0 DISSECTOR PERFORMANCE

In order to separate to the maximum degree possible the optical imaging problems, such as choice of optical aperture, lens speed, image size, etc. considered in Section 3.0 of this memo, from the tube detection problems proper, the input image geometry at the plane of dissector photocathode as shown in the following sketch will be assumed:

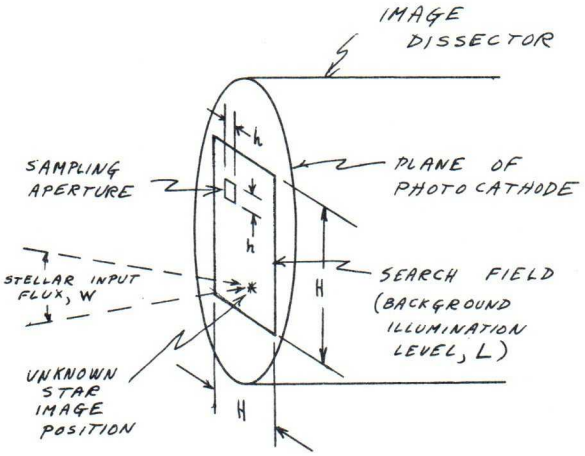

Figure 1 Image Field Parameters in Plane of Dissector Photocathode

It will also be assumed that an aperture or sampling element, h x h in size, is to be scanned electronically over the total search field area, H^2, in some programmed sequence, including all possible stellar flux locations. When the added flux, W, from the star to be located is detected in the output signal current from the dissector, the position of the aperture at that instant of time determines the unknown star position, terminating the search or acquisition mode. This search mode may then be followed by a tracking mode in which further position determination accuracy can be achieved and subsequent star motion followed through the field of view.

For simplification of this analysis, the usual continuous tv type raster line scan, will be assumed to be replaced by a jumped scan, in which each small image area, h x h, is observed for a small dwell time, t, and then the sampling aperture area, h x h, is jumped instantaneously to another (usually adjacent) area for the same time, t, etc. etc. This assumption of jumped scan is in fact quite rigorously applicable in theory, not only for image dissectors, but for other types of tv camera tubes (Ref. 1).

Because of the simplicity of image dissector action we can now write down the noise, signal, and signal-to-noise relationships as follows:

Where no star flux occurs, the aperture will collect a total number of electrons leading to an output count, n, during the dwell time, t, equal to

$$n = \epsilon L h^2 Q_{sk} t$$

where Q_{sk} is the quantum efficiency of the photocathode at the wavelength of the incident sky brightness photons involved (integrated over the spectral region involved), ϵ is the photoelectron counting efficiency of the dissector, and compatible units (See Section 4.2) are used for the various parameters.

If the number of counts, n, were exactly constant from one image element to the next there would, of course, be no difficulty in detecting a star, since, any increase in n, would mean an increased flux input, i.e. a star signal. Unfortunately this ideal situation never occurs, at least in the daytime, for there are always unavoidable sources of fluctuation in this background signal level during scan. In the limiting case, in which all fluctuations due to geometrical sky brightness variations, photocathode non-uniformities, photoelectron counting efficiency, etc. have been eliminated there will still be the fundamental statistical fluctuation of n (sometimes called background noise, shot noise, emission noise, etc.) which is proportional to the square root of n, i.e.:

$$\text{Statistical noise fluctuation} \cong \sqrt{n} = \sqrt{\epsilon L h^2 Q_{sk} t} \qquad (1)$$

For the image element which includes the stellar flux, W, the added electron count Δn for this element will be given by

$$\Delta n = \epsilon W Q_{st} t \qquad (2)$$

where it is assumed that all electrons from the star flux, W, enter the dissector aperture, and that Q_{st} is the quantum efficiency of the photocathode for the particular stellar flux spectral distribution involved.

The detection problem now resolves itself into detecting the change, Δn, in the counting rate due to the stellar flux over and above the random statistical fluctuations, $\sqrt{n}$. In other words a signal-to-noise ratio, S/N, can be expressed as:

$$S/N = (\Delta n)^2/n \qquad (3)$$

where the squared ratio is used in order to correspond more closely with the usual S/N power ratio. Substitution of the previously derived relationships Eq. 1 and Eq. 2 for Δn and $\sqrt{n}$ into Eq. 3 gives:

$$S/N = \frac{\epsilon W^2 Q_{st}^2 t}{L h^2 Q_{sk}} \qquad (4)$$

as the fundamental signal-to-noise ratio for a single interrogated image element.

If one assumes the most efficient search possible, i.e. where each element is interrogated or examined once and once only (no overlap of areas), then the available dwell time, t, is given by

$$t = \left(\frac{h}{H}\right)^2 T$$

where T is the total search time, divided equally among all searched elemental areas.

The S/N ratio then reduces to

$$\frac{S}{N} = \frac{\epsilon W^2 Q_{st}^2 T}{L H^2 Q_{sk}} \qquad (5)$$

This is the final relation for the S/N ratio in terms of dissector and image plane parameters. If one substitutes known values of the seven parameters appearing, the ability of the dissector to detect a specified star can be predicted from this equation. This prediction can be expected to be reasonably reliable (See Section 2.3).

Four of these parameters, the stellar flux, W, the permissible search time, T, the sky brightness background illumination, L, and searched area, H^2, are essentially predetermined by the conditions on the problem, i. e. the type of star, time of day, optics selected, etc. to be discussed in Section 3.0 of this memo. The principal dissector design parameters available for choice are the cathode quantum efficiencies, Q_{st} and Q_{sk} and counting efficiency, ϵ.

2.1 Choice of Dissector Aperture Size

It is quite surprising to note from Eq. 5 that, under the assumed conditions, the ability of an image dissector to locate the unknown star position is independent of the dissector aperture dimensions, h x h. The choice of aperture size must therefore depend on other system requirements, such as the desired star position accuracy. Surprisingly enough this positional accuracy can be as high as desired without a sacrifice in S/N ratio, within the assumptions of the problem.

One assumption is that the aperture must be large enough to collect all or nearly all of the photoelectrons from the stellar flux signal, W. In electrostatically focused star tracker tubes (actually low resolution image dissectors) such as the ITTIL FW-118, FW-129, FW-130, F4003, F4004, etc. the smallest practical paraxial size for the dimension, h, without loss appears at present to be about 0.005 inch, and this dimension increases rapidly off-axis (See ITTIL Applications Note E3). For magnetically focused dissectors such as the ITTIL FW-125, FW-146, F4010, F4011, and F4012, the minimum aperture size can be reduced to about 0.0005 inch to 0.001 inch on axis depending somewhat on permissible scan power, an improvement of about 50 to 100 times in positional determination accuracy without special tracking modes over the star tracker tubes. This reduced size can be maintained over comparatively large image areas. In terms of the resulting image fields of view for these various dissector tubes, these apertures represent star area locations within one part in 10^3 to 1 part in 10^7.

Another limitation is introduced by the necessity for some overlap between sampled target elements, for example between scan lines, in order to avoid loss of star signal at the boundaries between nominally adjacent elements. For very small apertures this overlap may lead to excessive percentage overlap, with resultant reduced S/N ratio.

Small apertures also require faster scan rates, wider bandwidths for the associated circuits, more scan power, greater circuit stability, etc. Other practical considerations in the choice of aperture size will include such parameters as sky brightness gradients, photocathode microstructure, etc. In general it appears that a combination of these secondary considerations will control the choice of aperture size rather than the S/N ratio.

2.2 Choice of Aperture Shape

The image dissector is quite unique in its adaptability to various aperture shapes. If desired, a rectangular aperture can be used, or even an aperture

with cross hairs or special reticles to introduce various signal selecting scan patterns. One example would be a "wagon wheel" type aperture, nutated electrically during scan to convert the usual star signal to a possibly-easier-to-process FM signal. It appears that these special techniques may allow closer approach to the limiting S/N ratio computed above than other less sophisticated methods.

2.3 Achievement of Limiting Sensitivity

The dissector performance computed herein is based on the assumption that the dissector can "see" and be limited by the statistical fluctuation of the background photoelectron emission count. Actually, this statistical count fluctuation is equivalent mathematically (Ref. 2) to the more commonly encountered shot noise law (Ref. 3):

$$i_n^2 = 2 e \mu k I_{dc} \Delta f \qquad (6)$$

where i_n is the anode noise current associated with an average anode current, I_{dc}, a bandwidth, Δf, the electronic charge, e, a multiplier gain, μ, and a multiplier noise factor, k. Multiplier phototubes, and the image dissector multiplier phototube in particular, are, in fact, capable of direct observation of this basic shot noise current, modified by the multiplier noise factor, k, (Ref. 3).

For "perfect" multipliers, the noise factor, k, is given by

$$k = \frac{\sigma}{\sigma - 1} \qquad (7)$$

where σ = the average gain/stage of the multiplier, giving, for $\sigma = 5$, $k = 1.25$, or a 25 percent increase in the noise. Thus "perfect" image dissectors should approach within about 80 percent of the S/N performance computed herein. In practice, we have shown that this close approach to limiting shot noise can be expected in properly designed tubes. The dissector, in fact, is quite unique among scanning detectors in this ability to "see" and be limited by the fundamental photoemission shot noise. While this fundamental noise may be excessive in dissectors for tv studio type applications, it does allow accurate analysis of expected dissector performance, as in this memo.

It should not be assumed, however, that all dissectors, regardless of design will approach the limiting performance. Dissectors with low gain multipliers, low current output capabilities, low photocathode average emission current density limits, or noisy electron multipliers may not achieve the S/N ratio computed herein. In particular, channel multiplier techniques, as opposed to discrete stage multipliers, do not presently appear to be capable of achieving the desired performance characteristics.

Surprisingly enough, there are sound technical reasons to believe that there are possibilities for new "smoothing multiplier" image dissectors in which the effective noise bandwidth, Δf, in Eq. 6 can be reduced, thus reducing the disturbing shot noise current, i_n, without loss of position determination accuracy, i.e. resolution. These new techniques, which hold considerable promise for advanced low noise image dissectors, are described in Ref. 11.

2.4 Dark Noise and Other Limitations

There may be other sources of disturbing "noise" in dissector systems, such as:

1. Photocathode inhomogeneities
2. Dark noise, either tube or circuit
3. Noise-in-signal (fluctuation of the actual flux to be detected)
4. Gain drift, etc.

H. Salinger, (Ref. 4) has shown that (2) and (3) are nearly always negligible for the daytime search or acquisition mode considered here. This follows from the high level of image background illumination normally encountered for daytime search. At night, or under tracking conditions as opposed to search, tube dark noise or noise-in-signal may be significant parameters. Gain drift, (4) can be expected to be negligible for the short acquisition times involved though it may present calibration problems. This leaves cathode inhomogeneities as a possible major source of false star acquisition. Experimental studies at ITTIL indicate clearly that these inhomogeneities can be markedly reduced and possibly made negligible by a simple improvement of cleanliness and cathode processing control procedures. Furthermore, most of these inhomogeneities have sizes, polarities, and shapes which are clearly not attributable to a star flux input. For maximum acquisition accuracy it will undoubtedly be necessary to choose discrimination circuits which reject inhomogeneities of improper size, shape, polarity, etc.

2.5 Multiple Aperture Dissectors

The above computation assumes one aperture and one electron multiplier. Multiple aperture dissectors with or without corresponding separate multipliers are feasible and have been constructed and tested at ITTIL. Such dissectors open up entirely new possibilities for star search, though the basic S/N computations from this memo can be modified for application to these more complex dissectors.

One particularly attractive possibility would be to use a dissector with two close-spaced apertures and

two separate electron multipliers, observing only the difference signal in the two output leads. This technique would effectively suppress gradual variations in sky brightness or photocathode sensitivity (i.e. shading).

It should be noted that this differential comparison technique is also possible with a conventional single aperture dissector, possibly at some cost of S/N ratio, by the use of a wobbled scan, i.e. a scan which has a small vertical scan motion superimposed onto the primary horizontal line scan. A differential star signal would then appear as an amplitude fluctuation at the wobbling frequency (moving off and on the star flux area during one cycle of the wobble frequency).

2.6 Complex Scan Techniques

Unlike ordinary tv camera tubes such as the image orthicon and vidicon in which a repetitive constant scan pattern is required to establish the proper charge storage, write, and read cycling operation, image dissector scan can be modified from time to time in any way desired without interference with the available signal output level. As a matter of fact the dissector scan can be stopped entirely and the tube operated in the dc readout mode as a high gain ultrasensitive multiplier phototube.

This versatility of scan choice allows considerable freedom in the selection of optimum scanning techniques. For example, one fast pre-scan raster might be used to locate the most probable star locations, followed by a slower detailed examination of these individual expected locations only, for positive identification of the element actually including the star flux input.

A related advantage of the dissector is that it is not sensitive to star image motion, which tends to smear the stored information in such devices, as the vidicon and image orthicon, and reduce both sensitivity and accuracy of image location. The image dissector can therefore be used with a single slow search scan, compared to the more rapid multiple scans needed for the vidicon-orthicon devices.

2.7 Noise Bandwidth and Related Parameters

The usual concepts of noise bandwidth, Δf, noise current, i_n, and dc current, I_{dc}, in the shot noise relationship, Eq. 6, have been bypassed, so-to-speak, in this analysis. These concepts are, of course, directly related to and can be derived from the statistical fluctuation, Δn, of the counting rate, n, if so desired, leading to the same results found herein (Ref. 2). There are certain "hidden" assumptions however, contained in this present anslysis which might be pointed out. For example, the bandwidth of the monitoring circuits must be wide enough to be able to distinguish between the signal counting rate, n_2, in one sampled element, from the signal counting rates, n_1 and n_3 in the preceding and following elements without "cross-talk" and without amplifier noise becoming significant. With fast scan rates (i.e. small apertures and short search times) this may involve circuit design problems.

2.8 Cathode Fatigue

Operation of any photoemissive surface exposed to daylight can lead to excessive emitted photocurrent with subsequent fatigue (loss of cathode sensitivity). In general the average emission current limit is about 1-10 $\mu a/cm^2$ if tube life is to be many hours. For the large "f" number lens usually used for star search (see numerical examples) and the short operating life (usually a few seconds), cathode fatigue should not be serious. For long time star tracking cathode illumination limits must be observed.

2.9 Maximum Anode Current

With the high gain multipliers required in order to count individual photoelectrons large dissector apertures at high light levels can lead to anode output current saturation. This space charge saturation limitation does restrict the choice of search aperture to the smaller values, but these are normally desired in any case for star location accuracy.

2.10 Counting Efficiency

The concept of counting efficiency as utilized herein is somewhat new to image dissector performance analyses, although it has been applied by several experimenters to ultra low noise multiplier phototube performance (see references cited in Ref. 6). In brief, the counting efficiency, ϵ, is just the ratio of the number of countable output pulses in the dissector anode circuit to the number of triggering photoelectrons. The output pulses may be individually counted, or they may be allowed to merge into the more usual fluctuating output current and appear as anode shot noise. For properly designed dissectors, absolute counting efficiency ratios as high as 0.8 to 0.9 can reasonably be expected. For the less well designed devices, noted in Section 2.3, this ratio may be quite low and represents a serious loss of sensitivity.

3.0 OPTICAL SYSTEM PERFORMANCE

In Section 2.0 of this memo, the characteristics of an image dissector for star acquisition were discussed, assuming certain image field characteristics in the plane of the photocathode. These image field characteristics are related to the viewed stellar field and the selected optical system as shown in Figure 2.

The image field illumination, L, is related to the sky "brightness", B, by the relationship:

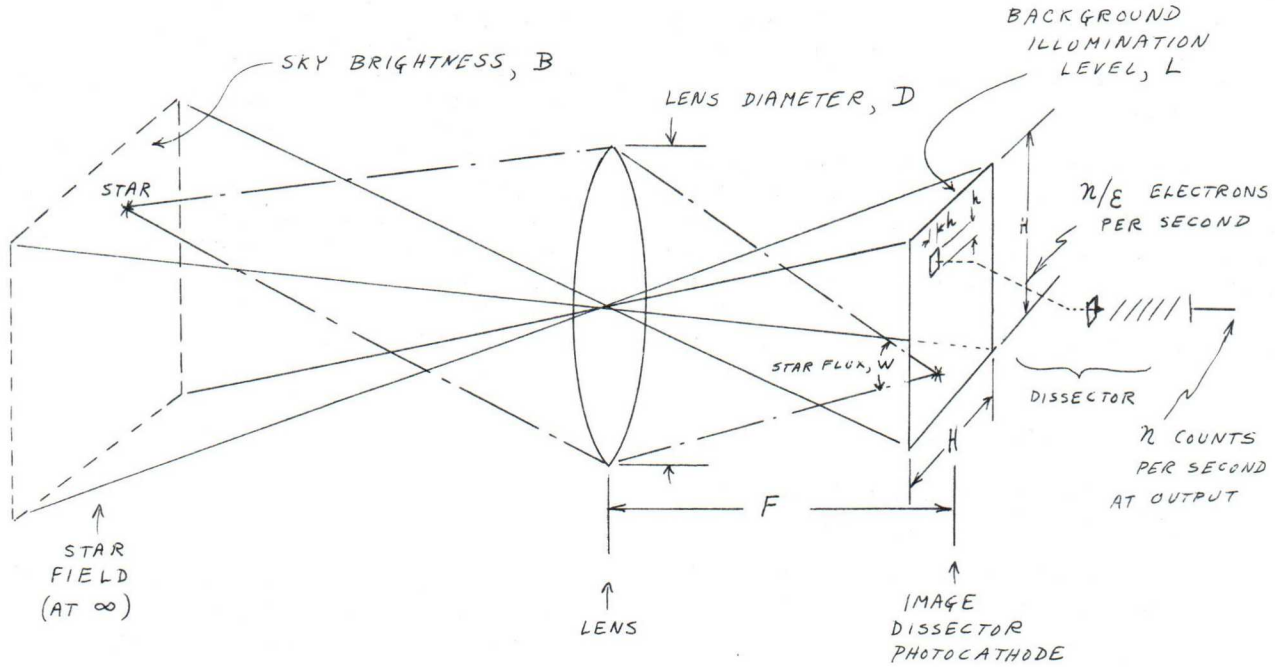

Figure 2 Optical Field Parameters

$$\frac{L}{B} = \frac{1}{4f^2} \quad * \qquad (8)$$

where f is the effective "f"/number of the lens. This "f"/number is, in turn, related to the effective lens diameter, D, and focal length, F, by the identity:

$$f = F/D \qquad (9)$$

In addition, the focal length F, is related to the field of view angle **, θ, and image field dimension, H, by:

$$\tan \theta/2 = \frac{H}{2F} \qquad (10)$$

or $$F \cong H/\theta \qquad (10a)$$

---

* This equation is numerically correct only if appropriate and corresponding paired units are used for "brightness", B, and illumination, L. Suitable pairs of units would be foot lamberts and foot candles, lamberts and phots, apostilbs and lux, etc., depending on the area units involved (ft^2, cm^2, and m^2 respectively). If true brightness units, such as candles/unit area or lumens/unit area/steradian, are used to express B, then the appropriate numerical factor of π must be included in Eq. 8.

** For simplicity the view field was assumed to be square in Figure 1. Other geometrics can of course be readily substituted.

Another simple relationship needed is that between the stellar image flux, W, and the stellar illumination level, I, at the plane of the optics, namely:

$$W = \frac{\pi D^2}{4} I \qquad (11)$$

Substitution of the above relationships into the S/N equation 5, gives for the fundamental S/N equation in terms of image dissector and stellar field parameters:

$$S/N = \frac{\epsilon (\pi DIQ_{st})^2 T}{4\theta^2 BQ_{sk}} \qquad (12)$$

A number of useful conclusions regarding the stellar acquisition problem can be derived from examination of this equation:

3.1 Choice of Optics

As far as the choice of optics is concerned the only directly appearing parameter in Eq. 12 is the effective lens diameter, D, which must clearly be as large as possible for maximum sensitivity. A secondary and hidden restriction in Eq. 12 is that the focal length of the lens must be chosen to yield the proper image field dimension, H, on the detector, for a given view angle, θ. As shown by the numerical examples listed later on in this memo, this restriction normally leads to a large focal length and rather surprisingly to a relatively "slow" lens speed, but larger or smaller detector fields can be selected without loss of sensitivity. Although lens "speed" does determine the background field illumination, L, the area, H^2, to be

searched by the image dissector also varies in such a way with fixed aperture diameter, D, as to just cancel out the change in noise with field illumination level due to a change in lens speed. Lens speed, per se, is therefore not a significant parameter or an image dissector star tracker.

Further restrictions on the choice of optics follow from the necessity that all of the star flux, W, must be focused to an area smaller than the selected dissector aperture size (but, of course, this aperture size choice itself is comparatively unrestricted, see Section 2.0), and the lens must yield the desired image quality as regards distortion, vignetting, aberrations, etc.

4.0 GENERAL OBSERVATIONS

4.1 Spectral Response, Filtering, and Cathode Quantum Efficiency Consideration

From Eq. 12 it follows that the effective star search sensitivity is proportional to the ratio

$$\frac{I^2 Q_{st}^2}{BQ_{sk}}$$

where the sensitivity products IQ_{st} and BQ_{sk} for stellar and sky flux respectively, contain all spectral response modifications due to selective atmospheric absorption, choice of photocathode, view angle with respect to the sun, etc. It has been suggested many times that selective optical filtering be used to improve the system performance by making use of the possibly small but unavoidable differences in spectral distribution which occur between stellar and sky brightness flux. However, since the product IQ_{st} enters as a squared parameter, while BQ_{sk} is linear only, it follows that it will usually be preferable in practice to maximize the sensitivity product, IQ_{st}, for the stellar flux, even though an apparent excess sensitivity, BQ_{sk}, to sky brightness flux may thereby result. This conclusion confirms the statement by Laverty (Ref. 5) that spectral filtering is seldom worthwhile in practice.

4.2 Choice of Units

Eq. 12 was derived on the basis of a certain numerical signal count per dwell time, t, compared to a certain statistical fluctuation count in the background count for the same dwell time. Eq. 12 must therefore be a dimensionless ratio based on numerical counting rates at the dissector output. The units of all parameters used in computing an S/N ratio from Eq. 12 must therefore be compatible with this counting concept. For example, if lumens, * centimeters, coulombs, and seconds are selected as the fundamental units, then the derived units listed in Appendix I must be used for the various parameters. The only unusual unit appearing in this system is the cathode quantum efficiency in electrons/lumen-second, in contrast with the more usual electrons/photon unit. However, cathode luminous sensitivity data in microamperes/lumen can be converted readily to the required values by dividing by 1.6×10^{-13}. Unfortunately μa/lumen cathode sensitivity figures are readily available only for input flux having a spectral distribution equivalent to a 2870° K color temperature tungsten lamp, which is hardly applicable to this stellar detection problem. Table I shows the computed ratio of luminous cathode sensitivity to the various spectral sources listed, compared to the standard 2870° K sensitivity for several JEDEC registered types of photocathodes.

* All commonly used photometric units can be expressed in terms of lumens plus the appropriate length, area and time dimensions.

TABLE I

Computed ratio of cathode luminous sensitivity (for the spectral distribution listed) to cathode luminous sensitivity (for 2870° K color temperature radiation).

Source	Type Photocathode S1*	S11*	S20*
5000° K black body	0.50	1.84	1.27
Mean solar flux	0.39	1.74	1.18
Daytime sky (Ref. 10)	---	---	1.91
P4* phosphor	0.11	1.94	1.12
P11* phosphor	0.16	5.4	2.74
P20* phosphor	0.083	0.69	0.51
NaI Scintillator (Harshaw data)	1.72	22.8	12.3

* Registered JEDEC spectral response distribution.

It can be seen that the luminous sensitivity of S-20 photocathodes is higher for "blue" sources, as usually encountered in stellar search problems.

4.3 Star Acquisition Versus Star Tracking

Upon first examination it might appear that star tracking (i.e. following a star as it moves through the field of view) is quite different from the star acquisition problem under consideration here, since, in star tracking, one can adopt a simpler scan pattern, such as the ITTIL rosette type scan (Ref. 7), in which one examines only a few "picture" elements surrounding the previously determined star location to see whether or not it has moved since the last scan.

However, since the S/N ratio in either mode is independent of the instantaneously examined element size, as noted in Section 2.1, there is inherently no difference in the two modes as far as application of the results of this analysis is concerned, though there may, of course, be numerical differences in the computed S/N ratio. In tracking modes in general, one will be dealing with only a few "picture" elements, a comparatively small* view field angle, θ and possibly a rather short repetition time, T, compared to acquisition modes, but, assuming that the appropriate numerical value of θ and T are substituted into the S/N Eq. 5 or 12, the ability to track as well as search, can be predicted. Both acquisition and tracking sensitivity is clearly proportional to T/θ^2:

$$S/N \text{ (track or search)} \sim T/\theta^2$$

It seems likely that the effective S/N ratio during track may be somewhat higher than indicated by the S/N equations computed herein, since there will be many repetitive scan frames involved, permitting frame-by-frame comparisons to help differentiate star signal from random noise.

5.0 NUMERICAL EXAMPLES

It is instructive to insert into the S/N Eqs., 5 and 12, some typical numerical data. To do this it is convenient to make use of the approximate relationship given by Allen (Ref. 8) between stellar magnitude, m, and star illumination, I, in lumens/cm^2 (i.e. phots):

$$I = 0.8 \times 2.65 \times 10^{-10} \times 10^{-0.4\,m} \qquad (13)$$

where a factor of 0.8 is included to correct for atmospheric absorption.

A further assumption will be that we are using an S-20 photocathode with a 150 μa/lumen sensitivity, so that the two effective cathode efficiencies Q_{st} and Q_{sk}, assuming we are tracking a star of the same spectral class as the sun, will be (using Table I):

$$Q_{st} = \frac{(1.18)\,(150)}{1.6 \times 10^{-19} \times 10^{6}}$$

$$= 1.1 \times 10^{15} \text{ electrons/lumen second}$$

$$Q_{sk} = \frac{(1.91)\,(150)}{1.6 \times 10^{-19} \times 10^{6}}$$

$$= 1.79 \times 10^{15} \text{ electrons/lumen second}$$

A final numerical assumption will be that an absolute counting efficiency ratio, ϵ, of 0.9 has been achieved (See Paragraph 2.10).

* During track, the star can be followed in general through a larger field of view, as limited by the dissector photocathode, gimbal movement, vehicle window etc.

With these assumptions the following specific cases are of interest:

5.1 General Star Search Problem (Laverty data, Ref. 5, page 195)

D = 2.5 inches = 6.35 cm

θ = 1/2° = 8.73×10^{-3} radians

W = 4.13×10^{-10} lumens

B = 300 ft. lamberts = 0.322 lamberts

These data give:

$$I = \frac{4.13 \times 10^{-10} \times 4}{\pi\,(6.35)^2}$$

$$= 1.26 \times 10^{-11} \text{ phots.}$$

Assuming an arbitrary search time of 1 second, Eq. 12 gives:

$$S/N = \frac{0.9 \times (3.14 \times 6.35 \times 1.26 \times 10^{-11} \times 1.1 \times 10^{15})^2 \times 1.0}{4 \times (8.73 \times 10^{-3})^2 \times 0.322 \times 1.79 \times 10^{15}}$$

$$\cong 0.4$$

This is not a useful S/N ratio; in other words, dissectors cannot be expected to acquire a star under the stated operating conditions. Relatively small changes in the operating conditions, such as an increase in the search time to 10 seconds, will, however, offer image dissector possibilities.

It might be noted that Laverty's comment, in Ref. 5, that "the ratio of the luminous energy from the sky background is five orders of magnitude higher than that from the star" in this example, while technically correct, is not a propos since the star flux is directed geometrically to a point image, while the sky brightness flux is distributed over the full search field area.

5.2 Vidicon Tracker, Laverty Data (Ref. 5 page 204)

D = 1.6 inches = 4.1 cm

θ = 15 ft = 4.4×10^{-3} radians

T = 0.25 sec (assuming one frame acquisition)

m = 2.19 (Polaris)

B = 400 ft. Lamberts = 0.43 lamberts

from which I = 2.85×10^{-11} phots and

$$S/N = \frac{0.9 \times (3.14 \times 4.1 \times 2.85 \times 10^{-11} \times 1.1 \times 10^{15})^2 \times (0.25)}{4 \times (4.4 \times 10^{-3})^2 \times 0.43 \times 1.79 \times 10^{15}}$$

$$\cong 0.62.$$

This numerical value is to be compared with the experimentally determined value of $(9)^2 = 81$ for the vidicon tracker listed by Laverty. It can be seen that the image dissector would not perform properly under these specific operating conditions. If the search time can be increased to 2.5 seconds the resulting S/N ratio of 6.2 would, however, offer significant possibilities.

5.3 Image Orthicon, Laverty Data (Ref. 5 page 204 - 205)

B = 1200 ft lamberts = 1.29 lamberts

θ = 13 ft = 3.8×10^{-3} radians

D = 2.37 inches = 6.02 cm

F = 64 inches = 162 cm

m = -3.1

T = 0.25 (one frame acquisition)

giving I = 3.64×10^{-9} phots and

$$S/N = \frac{0.9 \times (3.14 \times 6.02 \times 3.64 \times 10^{-9} \times 1.1 \times 10^{15})^2 \times 0.25}{4 \times (3.8 \times 10^{-3})^2 \times 1.29 \times 1.79 \times 10^{15}}$$

$$= 10,000$$

For a star as bright as this (-3.1 magnitude) it can be seen that the dissector should far exceed the capability of the image orthicon whose measured S/N ratio was $(6)^2 = 36$.

Recent successes in tracking the planet Venus under conditions almost identical with this example (Ref. 9) using an ITTIL dissector type star tracker (the FW-118) also confirm this conclusion.

5.4 Mechanical Tracker, Laverty Data (Ref. 5 page 203 - 204)

D = 2 inches = 5.1 cm

θ (track) = 2 ft = 5.8×10^{-4} radians

T (track) = 2 sec

m (gamma Gemini) = 1.93

B = 1200 ft. lamberts = 1.29 lamberts

giving I = 3.6×10^{-11} phots and

$$S/N = \frac{0.9 \times (3.14 \times 5.1 \times 3.6 \times 10^{-11} \times 1.1 \times 10^{15})^2 \, (2)}{4 \times (5.8 \times 10^{-4})^2 \times 1.29 \times 1.79 \times 10^{15}}$$

$$= 230$$

This computed S/N ratio compares favorably, as it should, since the dissector is merely a multiplier phototube with electronic scan, with the value of $(23.8)^2 = 570$ measured by Laverty for the mechanical scanner. An image dissector should in fact accomplish the same purposes as the mechanical scanner, but with greater system versatility and speed.

For the mechanical search mode reported by Laverty the time, T, was 10 minutes or 600 seconds and the search field angle θ was $1/2^o$ or 30 minutes of arc, giving

$$T/\theta^2 = 600/900 = 0.67$$

compared to

$$T/\theta^2 = 2/4 = 0.5$$

for the above track mode. Thus, a dissector should also perform both of these operations at approximately the same S/N ratio.

6.0 CONCLUSIONS

The image dissector appears to be capable of performance somewhat closer to that of competitive storage devices than may be apparent based on the ideal capabilities of these storage devices. While the dissector compares favorably with mechanical scanners, and exceeds the capabilities of the experimental image orthicon tracker cited, it does not compare favorably with the vidicon experimental tracker, at least for single frame acquisition. Whether or not slower frame times, multiple apertures dissectors, smoothing multiplier dissectors, image analysis techniques, FM modulation, or other specialized techniques can be used to improve dissector performance remains to be investigated.

REFERENCES

1. ITTIL Research Memo 246: "Photoconductive Camera Tube Theory".

2. ITTIL Research Memo by L. G. Wolfgang (to be published).

3. ITTIL Research Memo 309: "Noise in Multiplier Phototubes".

4. ITTIL Research Memo 397: "Star Tracking Limits of Performance".

5. N. P. Laverty "The Comparative Performance of Electron Tube Photodetectors in Terrestrial Space Navigation Systems", IEEE Tr. on Aerospace and Navigation Electronics, Vol. ANE-10, No. 3, September 1963, pages 194 - 205.

REFERENCES (Cont)

6. E. H. Eberhardt "Multiplier Phototubes for Single Electron Counting" paper presented at the Ninth Scintillation and Semiconductor Symposium, sponsored by the IEEE Prof. Group on Nuclear Science (to be published).

7. W. Atwill, Electronics, Sept. 30, 1960.

8. Allen "Astrophysical Quantities", 2nd Edition, 1963.

9. Project Balast, sponsored by the Air Force Cambridge Research Laboratories, under the direction of Prof. John Strong of Johns Hopkins University, Laboratory of Astrophysics.

10. R. K. H. Gebel, "Limitations for Daytime Detection of Stars Using the Intensifier Image Orthicon" Aerospace Research Laboratories Document ARL 64-46 Nov. 1963. (Conversion factor of 1.91 was computed from Curve XI, Fig 1, of this reference).

11. ITTIL Research Memo No. 398: "Smoothing Electron Multipliers".

APPENDIX I

LIST OF SYMBOLS AND APPROPRIATE UNITS*

B = sky brightness (lamberts)

D = effective diameter of optical system (cm)

f = "f"/number of optical system

F = focal length of optical system (cm)

h = dimension of one side of instantaneous sampling aperture (cm) (h x h area)

H = dimension of one side of image field at photocathode (cm) (H x H area)

I = illumination due to star at entrance aperture of optical system (phots)

L = image field illumination due to sky background brightness (phots)

n = number of photoelectrons per sampling time (sec^{-1})

Δn = increase in n due to star flux signal (sec^{-1})

t = sampling time per element (sec)

T = total search or frame time (sec)

W = star flux at photocathode image plane (lumens)

Q_{st} = effective quantum efficiency of photocathode for star flux (electrons/lumen second)

Q_{sk} = effective quantum efficiency of photocathode for sky brightness background flux (electrons/lumen second)

θ = viewed field angle (radians) (θ x θ total field)

e = electronic charge (coulombs)

I_{dc} = average dc current (amperes)

Δf = bandwidth (sec^{-})

i_n = noise current (amperes)

σ = average gain/stage of multiplier

k = multiplier noise factor

m = stellar magnitude

S/N = signal-to-noise power ratio

ϵ = absolute dissector counting efficiency ratio.

---

* (Based on a lumen, centimeter, coulomb, second system).

RESEARCH MEMO NO. 386

SIGNAL-TO-NOISE RATIO IN IMAGE DISSECTORS

Prepared by

E. H. Eberhardt

The comparatively noise-free current amplification properties of the electron multiplier used in image dissectors makes it possible to observe directly in the output circuit the random shot noise present in the photocathode emission current. This shot noise obeys the familiar "white" noise law:

$$i^2_{nk} = 2e\, I_k\, \Delta f$$

where i_{nk} = rms noise current (amps) at the photocathode

e = electronic charge = 1.6×10^{-19} coulombs

I_k = d-c current (amps) at the cathode corresponding to i_{nk}

Δf = bandwidth (cps)

Following current amplification by a factor, u, in the electron multiplier, such that:

i_{na} = rms anode noise current (amps) = ui_{nk}

and I_a = d-c anode current (amps) = $u\, I_k$

the above relationship reduces to:

$$i^2_{na} = 2\, e\, u\, I_a\, \Delta f\, \sigma/(\sigma - 1)$$

where σ = effective gain/stage in the early stages of the electron multiplier. (The above considerations are discussed in more detail in Research Memo No. 337: "Noise in Image Dissector Tubes", and in Research Memo No. 309, "Noise in Multiplier Phototubes".)

The d-c anode current, I_a, as well as the corresponding rms anode noise current, i_{na}, can be a result not only of photoemission but also of thermionic emission and other dark current sources from the photocathode. However, for the purposes of this memo all dark current sources other than photoemissive will be disregarded since, as shown in Appendix B, the photocurrents necessary for reasonable signal-to-noise performance in tv-type operation completely surpass any possible dark current in presently available photocathodes. Under these conditions the d-c current, I_a, can be considered as a signal current and a signal current-to-rms noise current ratio, $(S/N)_{rms}$ can be defined as:

$$(S/N)_{rms} = I_a/i_{na} = \sqrt{\frac{I_a\,(\sigma - 1)}{2\,e\,u\,\sigma\,\Delta f}} = \sqrt{\frac{I_k\,(\sigma - 1)}{2\,e\,\sigma\,\Delta f}}$$

This equation can be reduced to a more useful approximate form by making the following simplifications.

First, the cathode current, I_k, is given by:

$$I_k = J_k\, a/m^2$$

where a = dissector defining aperture area (cm^2)

J_k = d-c cathode current density ($amps/cm^2$)

m = linear magnification, cathode-to-defining aperture.

Secondly, the bandwidth, Δf, will be assumed to be no greater than absolutely necessary to "see" a resolution element during scan. This is equivalent to "allowing" one-half cycle i.e. a half wavelength, per aperture dwell time, Δt, or:

$$\Delta t \cong \frac{1}{2\,\Delta t}$$

The "dwell time", Δt, is essentially the time permitted to remain on one element if a continuous scan were to be replaced by a step scan in which the scan is jumped instantaneously between contiguous resolution elements. Possible overlap considerations, as in the case of round elements, as well as aperture correction techniques are ignored herein since the above relationship in any case is only approximate.

Thirdly, the rms noise current used above is not a good measure of visible noise in an image presentation, a more useful noise magnitude being the "peak-to-peak" value.

While "peak-to peak" measurements are basically meaningless with random noise of the type under consideration,[1] nevertheless, in practice, an approximate peak-to-peak amplitude i_n (peak-to-peak) can be estimated visually from an oscilloscope presentation. Experimental correlations made in our lab, as well as theoretical noise considerations,[2] lead to the following approximation:

$$i_n \text{ (peak-to-peak)} \cong 7 \; i_n \text{ (rms)}$$

With the above three simplifications, the effective signal current-to noise current ratio, $(S/N)_{eff}$, becomes

$$(S/N)_{eff} \cong \frac{1}{7} \sqrt{\frac{J_k \; a \; \Delta t \; (\sigma - 1)}{m^2 \; a \; \sigma}}$$

For a given dissector design the effective signal-to-noise current ratio is proportional to

$$(S/N)_{eff} \sim \sqrt{J_k \; a \; \Delta t} = \sqrt{\text{cathode current density x aperture area x dwell time}}$$

Figure 1 shows a plot of $(S/N)_{eff}$ vs J_k for various values of the parameter "$a\Delta t$". The two dotted lines on this graph show the calculated characteristics of (1) an image dissector with a 3-inch diameter photocathode and a 5-mil aperture operated at standard tv scan rates (giving 360 tv-line resolution for a theoretical 100 percent modulation factor), and (2) an image dissector with a 1-inch diameter cathode, a 1-mil aperture, and an 8-cps horizontal readout rate (giving 600 tv-line resolution). The loss of S/N ratio expected in going from 5 mils to 1 mil is more than compensated for by the much slower scan rates in the second dissector, the end result being much better S/N ratio.

The first dissector is only marginal in performance at standard tv rates, the S/N ratio at the minimum safe cathode current density of 1 $\mu a/cm^2$ being only 1.3. This corresponds well with experimental evidence. The S/N performance can be and has been improved by increasing the cathode illumination and thus the current density, J_k, but this usually is possible only at the expense of shortened tube life due to irreversible photocathode fatigue.

Unfortunately, definitive data on permissible cathode emission current densities is not yet available experimentally. It varies from tube to tube, with the permissible fatigue permitted during tube life, and with the type of photocathode.

---

1 Noise pulses of any given magnitude always have a finite probability of occurring.

2 See, for example, Bell System Technical Journal, Volume 24, p 74.

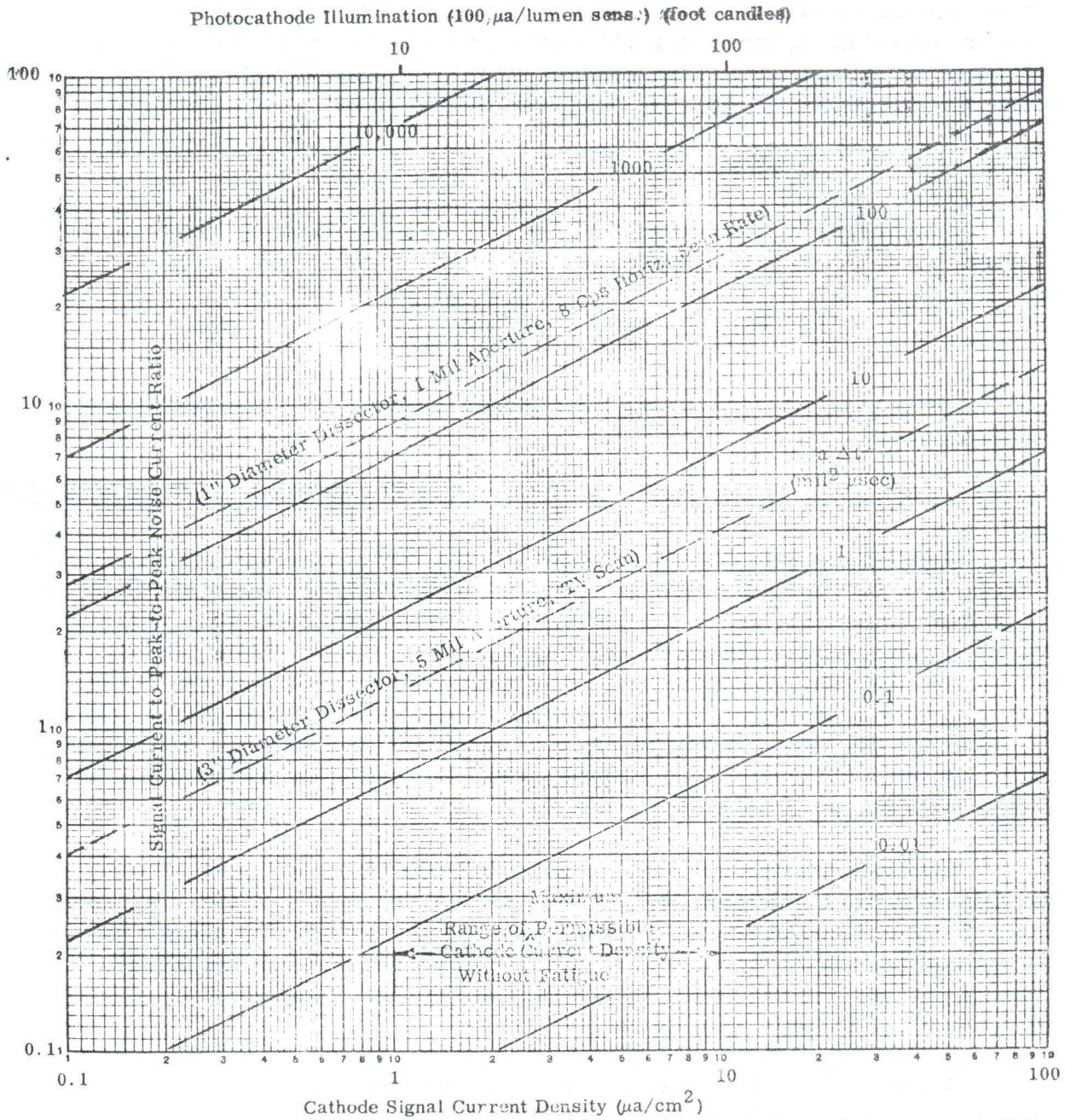

Assumptions:

i (noise, peak-to-peak) ≅ 7 i (noise, rms), SE ratio ≅ 2.6, I(dark) ≪ I (signal), $\Delta f \cong \frac{1}{2\Delta t}$

Figure 1 Calculated Image Dissector Performance Characteristics

The above relationships show that the S/N ratio is not a function of cathode sensitivity or quantum efficiency provided sufficient input flux density can be provided to supply a fixed emission current density, J_k. This is quite contrary to the usual threshold type considerations where the input flux is limited in magnitude and the S/N ratio is therefore proportional to the square root of the cathode sensitivity.

Figure 2 shows a conversion type plot for computing the performance parameter "a Δt" from known system parameters. The basis for this figure is given in Appendix C. The two specific image dissector examples shown in Figure 1 are also shown in Figure 2.

In summary, the S/N performance of image dissectors limits them to applications in which high illumination levels[3] and/or slow scan rates occur. They do have the following advantageous characteristics:

a. high resolution, approaching 1000's of tv lines[4]

b. excellent linearity over a wide dynamic range, the output current being directly proportional to the input flux over many orders of magnitude.

c. variable scan rates, including stopped scan (d-c read-out), random access, etc.

d. operable with rapid camera panning

e. simplicity of design, with no electron gun

f. rugged construction principles, suitable to special environments

g. wide range of permissible operating temperatures, limited only by photocathode damage of high temperatures

h. fast response, of the order of nanoseconds

i. the ability to see random shot noise of the input radiation image, i.e. "background noise limited" operation.

j. readily calculable signal-to-noise characteristics, permitting accurate system pre-evaluation studies.

---

3 A specialized technique for providing very high illumination levels without exceeding the average cathode current density limits has been described by Dr. G. Papp in ITTIL Research Communication No. 36 "On a Novel Application of the Image Dissector".

4 The limiting resolution of image dissectors has been treated by Dr. G. Papp in detail (IRE Trans. on Nuclear Science Vol NS-9 No. 2 p. 91-93, April 1962).

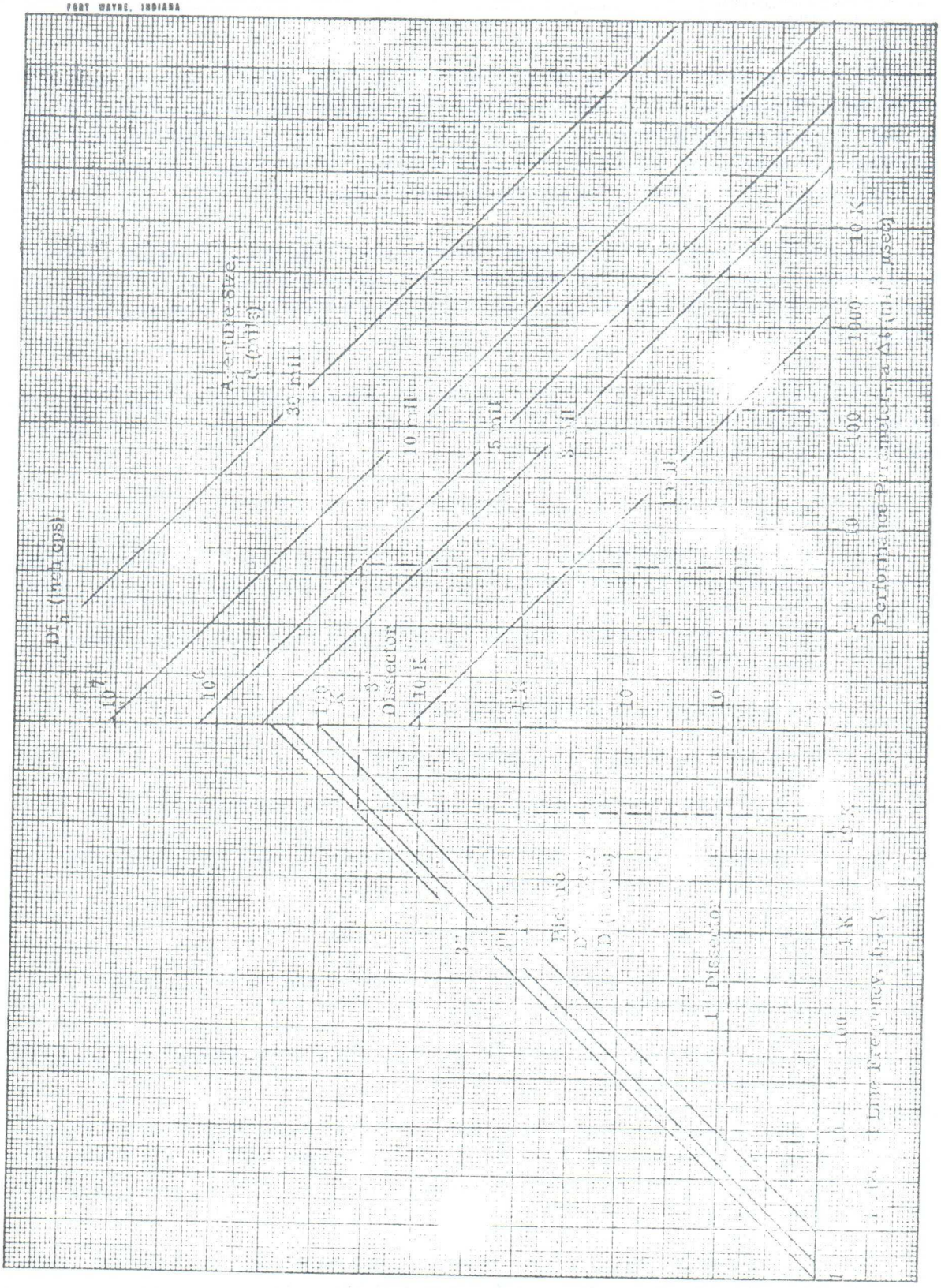

Figure 2 Dissector Dwell Time Characteristics

APPENDIX A

NUMERICAL CALCULATIONS

In plotting Figure 1 the following numerical data was used:

m = image magnification = 1

e = charge on the electron = 1.6×10^{-19} coulombs

σ = gain/stage = 2.6 (a typical value)

J_k (amps/cm^2) = J_k (μa/cm^2) $\times 10^{-6}$

a (cm^2) = a (mil^2) $\times 10^{-6} \times (2.54)^2$

Δt (sec) = Δt (μsec) $\times 10^{-6}$

giving

$$(S/N)_{eff} \cong \frac{1}{7}\sqrt{\frac{J_k\,(\mu a/cm^2) \times 10^{-6} \times a\,(mil^2) \times 10^{-6} \times (2.54)^2 \times \Delta t\,(\mu sec) \times 10^{-6} \times 1.6}{(1) \times 1.6 \times 10^{-19} \times 2.6}}$$

$$\cong 0.7\sqrt{J_k\,(\mu a/cm^2)\; a\,(mil^2)\; \Delta t\,(\mu sec)}$$

This is the equation plotted in Figure 1.

Example 1:

For an image dissector with a 5-mil aperture, 3-inch cathode diameter, and operated at standard tv rates.

a = 25 mil^2 (assuming a square aperture)

Horizontal line length $= (4/5) \times 3'' = 2.4'' = \frac{2.4}{0.0005} = 480$ apertures/line

Horizontal line time $= \frac{1}{15{,}500}$ sec $= 64.5$ μsec (neglecting retrace time)

$$\Delta t = \frac{64.5}{480} = 0.134 \ \mu sec$$

$$a\Delta t = (25)(0.134) = 3.36 \ mil^2 \ \mu sec$$

$$(S/N)_{eff} = 1.28 \sqrt{J_k (\mu a/cm^2)}$$

Example 2:

For an image dissector with 1 mil aperture, 1-inch photocathode diameter, and 8-cps horizontal scan rate, the corresponding numerical data is:

$$a = 1 \ mil^2 \quad \text{(assuming square aperture)}$$

Horizontal line length $= 4.5 \times 1'' = 0.8'' = \frac{0.8}{0.001} = 800$ apertures/line

Horizontal line time $= 1/8 = 0.125$ sec $= 125,000 \ \mu sec$

$$\Delta t = \frac{125,000}{800} = 156 \ \mu sec$$

$$a\Delta t = 156 \ mil^2 \ \mu sec$$

$$(S/N)_{eff} \cong 8.7 \sqrt{J_k (\mu a/cm^2)}$$

APPENDIX B

DARK CURRENT MAGNITUDES

An examination of Figure 1 shows that relatively large cathode current densities (above at least 0.1 $\mu a/cm^2$) are required if usable signal-to-noise ratios are to be achieved with image dissectors at "ordinary" raster scan rates. These required current densities are many orders of magnitude greater than dark current densities experienced even with S-1 photocathodes (whose maximum dark current density is seldom greater than 10^{-5} $\mu a/cm^2$). Thus photocathode dark current and dark current noise is never significant in ordinary dissector applications,[5] The limiting tube noise is therefore noise in signal under all ordinary conditions, i.e. random fluctuations of the signal itself.

If, however, large apertures and/or very slow scan rates occur, as in star tracking applications using such simplified tubes as the FW118, FW129, and FW130, then dark noise can be and is, in fact, usually encountered.

Photocathode thermionic emission dark current and dark noise can be included directly in the above computations if so desired, by merely replacing I_k in Equation 1 by a combined term, $I_{thermionic} + I_{photoemission}$, and carrying this sum, or its equivalent, throughout the remaining performance equations.

5 Of course, other types of dark current and dark noise may occur in some cases, such as amplifier noise, leakage, pickup, etc.

APPENDIX C

DWELL TIME CONSIDERATIONS

The dwell time, Δt, and the product, $a\Delta t$, have interesting and rather complex physical significance. Dimensionally, $a\Delta t$ is in cm^2 sec or the equivalent. Physically it is equal to the amount of charge gathered per one element sample per unit cathode current density.

Under many conditions, when the aperture area, a, is decreased, the dwell time, Δt, must also be decreased (in order to allow time to scan the larger number of picture elements). For example, if the scan rates are fixed and the aperture diameter is reduced to 1/10 of its original size, the dwell time is also down by 1/10, "a" is down by 1/100, "$a\Delta t$" is reduced to 1/1000 of its original amplitude, and the S/N ratio is down by 1/31.4. This is a greater loss of performance than is directly apparent from the performance equations. Furthermore, with the smaller aperture, the number of horizontal lines should be increased (by 10 x in the above case) to make full use of the improved resolution. If this were done the end result for a fixed frame time would be a signal-to-noise current ratio down to 1/100 of its original value.

For the usual tv type application, with a 4 to 3 raster geometry inserted within a picture (photocathode) diameter, D, a horizontal line frequency, f_n, and a square aperture of side, d, the product, $a\Delta t$, is given by

$$a\Delta t = \frac{5d^3}{4Df_h} \quad (cm^2 \text{ sec})$$

$$a\Delta t \ (mil^2\ \mu sec) = \frac{5 \times 10^{-3}}{4} \quad \frac{d^3\ (mil^3)}{D(in)\ f_h\ (mc)}$$

This is the relationship used in plotting Figure 2.

RESEARCH MEMO NO. 337

NOISE IN IMAGE DISSECTOR TUBES

By

E. H. Eberhardt

May 1, 1961

Noise in image dissector tubes may be divided into two general classifications: (1) spurious noise which can be avoided or minimized by careful design, and (2) fundamental noise which cannot be avoided.

Spurious noise may be caused by ion feedback, hum pickup, deflection coil current pickup, etc., and can be expected to be low in amplitude in a properly designed and properly operated tube.

Fundamental noise, on the other hand, is inherently present and must be considered in any practical dissector application. Fortunately, the theory of the dissector tube is so simple that it is relatively easy to compute the fundamental noise limitations.

The fundamental noise can be divided into three types: (1) statistical fluctuation of the dark current, i.e. thermonic emission from the photocathode (2) statistical fluctuation of the signal current emitted from the photocathode as a result of a flux input signal, and (3) statistical fluctuations of the secondary emission multiplication process in the multiplier dynodes.

Noise from the first two sources can be computed from the well known shot law:

$$i_{nk}^2 = 2 e I_k \Delta f$$

where

I_k = The d-c current entering the dissector defining aperture, emitted from a corresponding photocathode area as chosen by the deflection fields and aperture size.

i_{nk} = rms noise component of I_k

e = charge on the electron = 1.6×10^{-19} coulomb

Δf = noise bandwidth in cps

If I_k is the magnitude of the dark current, then i_{nk} is the dark noise current; if I_k is the signal current only, then i_{nk} is the so-called noise-in-signal current; and if I_k is the total current, i_{nk} is the total noise current.

For most dissector applications the dark current and dark noise current are both negligible compared to the signal current and noise-in-signal current and can be neglected. However, for some applications it is convenient to know that the dark (thermionic) emission from an S-1 photocathode normally lies between 3×10^{-13} and 3×10^{-12} amperes/cm^2 and for an S-11 or an S-20 photocathode it normally lies between 10^{-15} and 10^{-14} amperes/cm^2. These figures will permit a dark noise current estimation if desired.

Considering now the multiplier anode output circuit, the d-c anode current, I_a, is derived from the d-c cathode current, I_k, by multiplying by the current amplification, μ, of the electron multiplier structure, thus:

$$I_a = \mu I_k$$

where the subscript "a" refers to the multiplier anode output circuit.

The corresponding noise current in the anode circuit, i_{na}, is obtained by multiplying the cathode noise current, i_{nk}, by two factors: first, the current amplification, μ, and second, the factor $[\sigma/(\sigma-1)]^{1/2}$ where σ is the gain/stage of the electron multiplier[1]. This latter factor accounts for the third type of fundamental noise listed previously, namely that due to fluctuations of the secondary emission ratio.

The anode circuit noise current is then

$$i_{na} = \mu \left[\frac{\sigma}{\sigma-1}\right]^{1/2} i_{nk}$$

---

1 See, for example, Spangenberg, "Vacuum Tubes", McGraw Hill Book Company, New York, 1948, p 320 ff. With $\sigma \cong 3$ in the usual ITT multipliers, the noise increase due to secondary emission is $[3/2]^{1/2} = 1.22 = 22\%$.

and the relationship between i_{na} and I_a is

$$i_{na}^2 = 2e\mu I_a \Delta f \sigma/(\sigma - 1)$$

Comparing this final equation for anode noise current with the basic shot law shows that anode noise in a dissector tube acts as if it were shot noise generated by unit charges having an amplitude of

$$e \mu \sigma/(\sigma - 1)$$

or approximately μ times the unit charge, e. This is an easy way to remember the relationship for anode circuit noise.

In an actual operating dissector all of the necessary parameters above can be readily determined experimentally with the exception of the noise bandwidth, Δf. This bandwidth may be estimated from the approximate relationship

$$\Delta f \simeq (1/2 \Delta t)$$

where

Δt = time taken to scan across one single aperture width.

It can be seen that dissector noise varies as the square root of the scan speed, i.e. as the square root of the scan frequency for a given scanned area. Slow scan speeds are necessary for low noise and clearly a compromise must always be made between resolution and signal-to-noise ratio.

Further discussions of dissectors or dissector-type operation may be found in the references on the following page.

BIBLIOGRAPHY

1. "Reference Data for Radio Engineers", International Telephone and Telegraph Corporation, 4th Edition, 1949, p 410 ff.

2. Zworykin and Morton, "Television", John Wiley and Sons, Inc., New York 1940 p 230 ff.

3. Spangenberg, "Vacuum Tubes", McGraw Hill Book Company, New York, 1948, p 729.

4. P. T. Farnsworth, "Television by Electron Image Scanning", J. Franklin Institute, vol 218, pp 411-444, October 1934.

5. H. Salinger, "The Electrostatic Image Dissector", Proceedings of the National Electronics Conference, Vol. 2, 1946, pp 1-7.

6. D. G. Fink, "Television Engineering", McGraw Hill Book Company, New York, 2nd Edition, 1952, pp 95-99.

7. C. C. Larson and B. C. Gardner, "The Image Dissector", Electronics, 12 (10): 24 (October 1939).

8. J. K. Belovich, "The Image Dissector", ITT Research Memo 316.

9. E. H. Eberhardt, "Noise in Multiplier Phototubes", ITT Research Memo 309, November 8, 1960.

10. E. H. Eberhardt, "Thermionic Emission in Multiplier Phototubes", ITT Research Memo 311, November 4, 1959.

RESEARCH MEMO NO. 336

IMAGE DISSECTOR TUBE

by

J. F. Belovich

April 28, 1961

The first television camera tube, the image dissector, was invented and developed by Philo T. Farnsworth of the Farnsworth Electronics Company in 1934. It was the first successful non-mechanical system of scanning to be in operation.

The features of the Farnsworth image dissector are shown in Figure 1. Essentially, the tube consists of a translucent cathode, the surface of which is coated with photo-sensitive material, and upon which is projected the optical image of the scene to be transmitted. This optical image causes a photo-emission of electrons which are distributed in space with a density at each part of the cathode plane proportional to the light intensity of that particular part of the picture. The electron-optical image is then propelled from the cathode to the anode by means of an electrical field. Proper focusing is achieved with the aid of a uniform axial magnetic field. The distribution of electrons at the anode plane corresponds to the distribution of light intensity upon the cathode, thus giving at the anode what might be termed an electron image of the scene being reproduced. The anode is perforated in the center by a tiny aperture behind which is an electrode which collects the electrons passing through the aperture. This electrode, the first dynode, receives an electron current proportional to the light intensity of the corresponding part of the optical image. The picture is scanned by displacing the electron image at the anode with respect to the aperture so that the part of the image that supplies electrons to the first dynode is continuously changing in a systematic manner so as to measure the light intensity of each elemental part of the entire projected scene. This is achieved by deflecting the whole electron image in two directions at right angles to each other with the aid of two magnetic fields which are produced by two pairs of coils as shown in Figure 2. The electron current received by the first dynode through the aperture has an instantaneous value equal to the photocurrent from a single element of the cathode. It has been calculated that under ordinary conditions a bright outdoor scene gives only a few hundred electrons from an elemental cathode area equal to the aperture area as it is scanned. This amount of signal current is so small that, if it were amplified, thermal-agitation voltages in the input circuit of the first tube would be comparable to the signal.

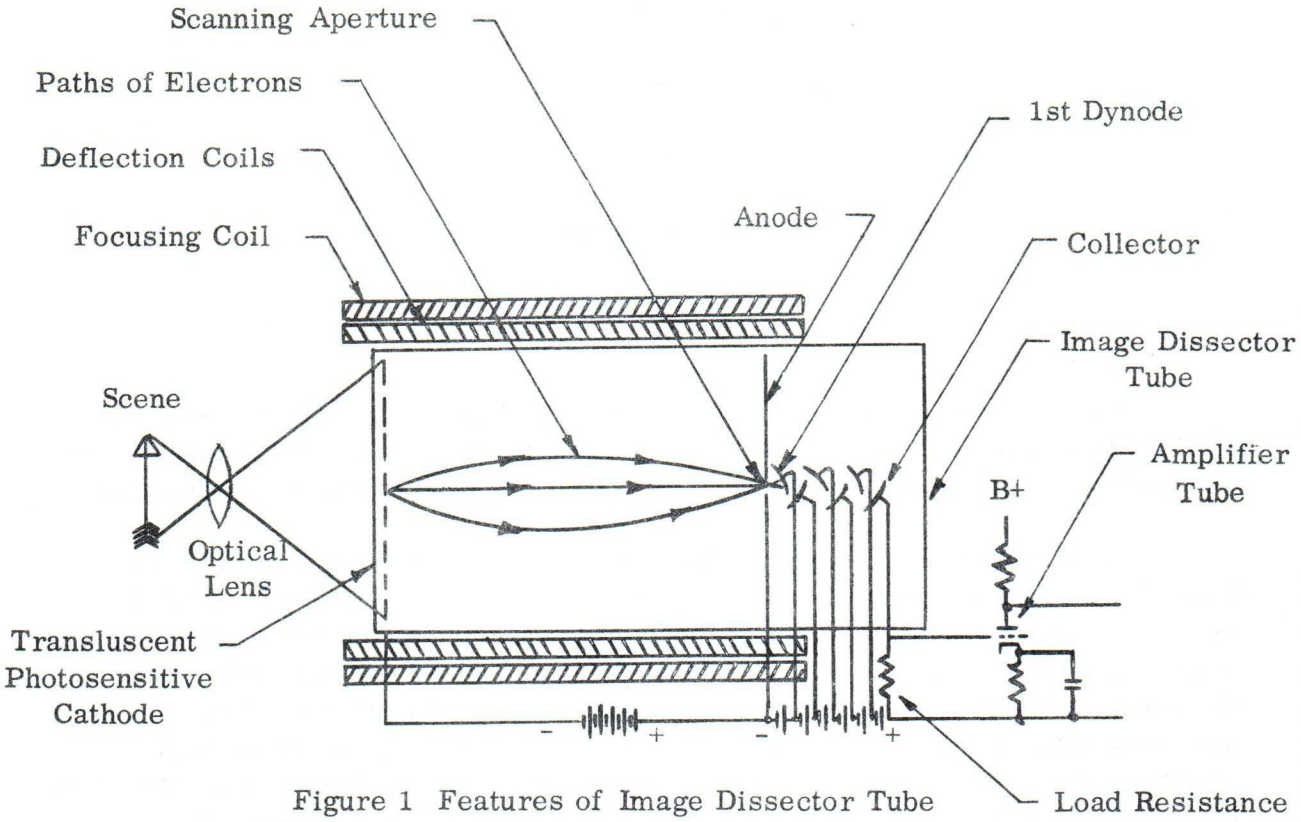

Figure 1 Features of Image Dissector Tube

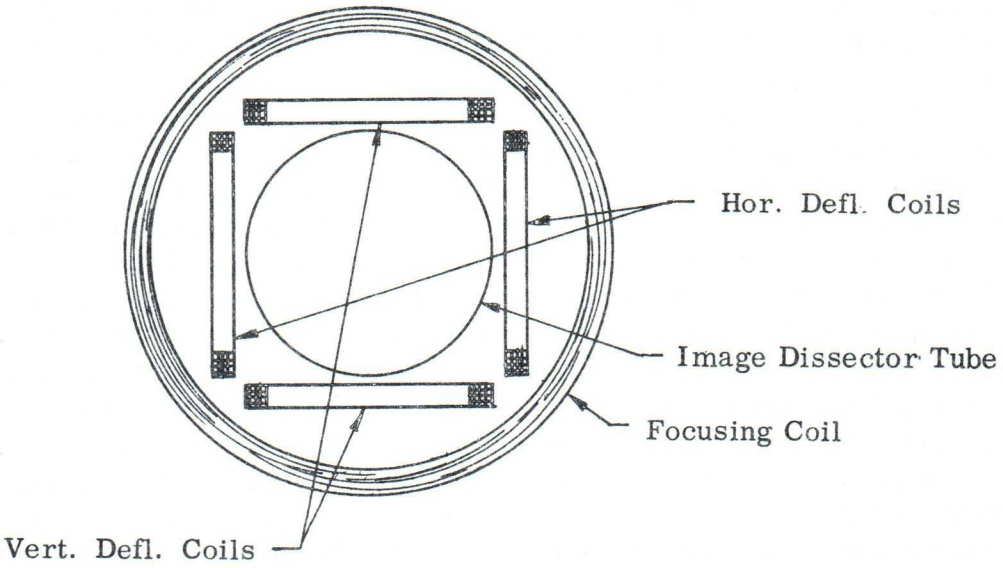

Figure 2 Focusing and Deflection Coils (End View)

This limitation has been overcome by making use of secondary emission to multiply the number of electrons that the scanning tube develops. Several dynodes are incorporated in the multiplier section to build up the small signal current to a value that can be made distinguishable. The result is a reproduced picture of higher contrast.

In order to account for the experimental facts observed in connection with the phenomenon of photoemission, it is necessary to make use of the quantum theory of radiation, as well as the quantum mechanical picture of metals. This paper is too brief to include an adequate discussion of this subject. There are several good books which cover this subject thoroughly, and as a starter, reference is made to Television by Zworykin and Morton, pp. 22-28.

Various physical phenomena occur when electrons are in the vicinity of an electric and/or a magnetic field. The rest of this paper will be a discussion of the various influences by these fields on the electrons in the image dissector tube from the time they are released at the photocathode until they are removed from the multiplier output as a video signal.

In order to understand just how the axial magnetic field influences the moving electrons for proper focusing, the orbit of a charged particle in a magnetic field must be understood. Let a negatively-charged particle at point 0 in a uniform magnetic field of flux density B be given a velocity v in a direction at right angles to the field. (See Figure 3.) An upward force F, equal to Rev, is exerted on the particle at this point. Since the force is at right angles to the velocity, it will not affect the magnitude of this velocity but will merely alter its direction. At points such as P and Q the directions of force and velocity will have changed as shown, the magnitude of the force remaining constant. The particle therefore moves under the influence of a force whose magnitude is constant but whose direction is always at right angles to the velocity of the particle. The orbit of the particle is therefore a circle described with constant tangential speed v, with force F being the centripetal force. Since

$$\text{centripetal acceleration} = \frac{v^2}{r}$$

we have from Newton's second law,

$$Bev = \frac{mv^2}{r}$$

and the radius of the circular orbit is

$$r = \frac{mv}{eB}$$

Notice from the above equation that the radius of this circle is smaller the greater the strength of the magnetic field and the more slowly the electron is moving through the field.

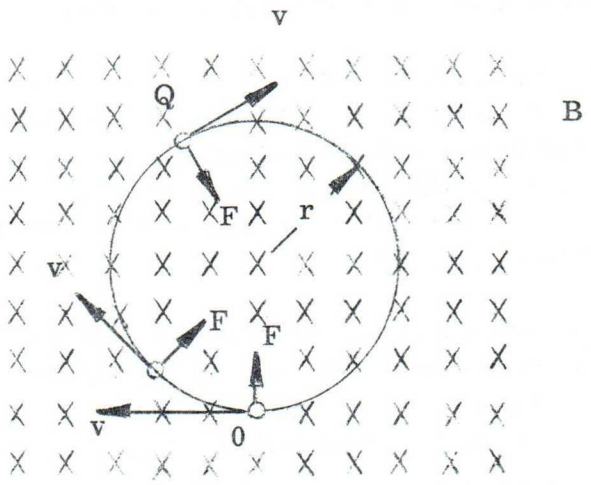

Figure 3 Circular Orbit of an Electron in a Uniform Magnetic Field

If the direction of the initial velocity is not perpendicular to the field but at some angle to it, the particle moves in a helical path. When an electron moves exactly parallel to the direction of the lines of induction of a magnetic field, no force is exerted upon it and it continues unchecked in its course. But, if there is the slightest difference in direction, the velocity v of the electron may be considered to be split up in a direction parallel to the lines of induction and in a direction perpendicular to those lines. The perpendicular component is affected by the magnetic field as though the axial component were non-existent. If the angle made by the path of the electron with the lines of induction when entering the magnetic field is x, the axial component is $v_1 = v \cos x$ and the radial component $v_2 = v \sin x$. As a result of this radial component, the projection of the electron on a plane perpendicular to the lines of induction will be a circle with radius:

$$r = \frac{m v_2}{e B} = \frac{m v}{e B} \sin x.$$

The path of the particle is therefore a spiral line on a cylinder with its axis parallel to the lines of magnetic induction. If, therefore, a number of electrons coming from a point P on the cathode enter the axial magnetic field at different angles, all the particles will describe helical paths according to the above equation, but each path will have a different radius. Since the line of induction through the point P on the cathode is a common denominative of the cylinders forming the surrounds of the spirals described by the electrons as shown in Figure 4, the electron is more or less compelled to follow the lines of induction; the greater the magnetic induction, the closer they follow the lines.

The transit time T for one revolution round the cylinder is

$$T = \frac{2\pi r}{v_2} ,$$

and since

$$v_2 = \frac{eBr}{m} ,$$

after substitution it follows that:

$$T = \frac{2\pi m}{eB} .$$

In other words: in the same interval of time and regardless of the angle x, each electron will describe a complete circle, of which the radius is a function of x. In that time the distance travelled by the electron in the direction of the field is:

$$T v_1 = \frac{2\pi m}{eB} v \cos x.$$

If, therefore, the electrons contained in an electron beam leave a common point at the same speed v but at small angles to the direction of the lines of magnetic induction of the uniform field, the axial distance travelled will be the same for all the particles as long as the angle x is so small that it may be assumed, with sufficient accuracy, that cos x = 1. Although the separate particles leaving point P of the cathode describe spirals on cylindrical planes with different radii, they all converge

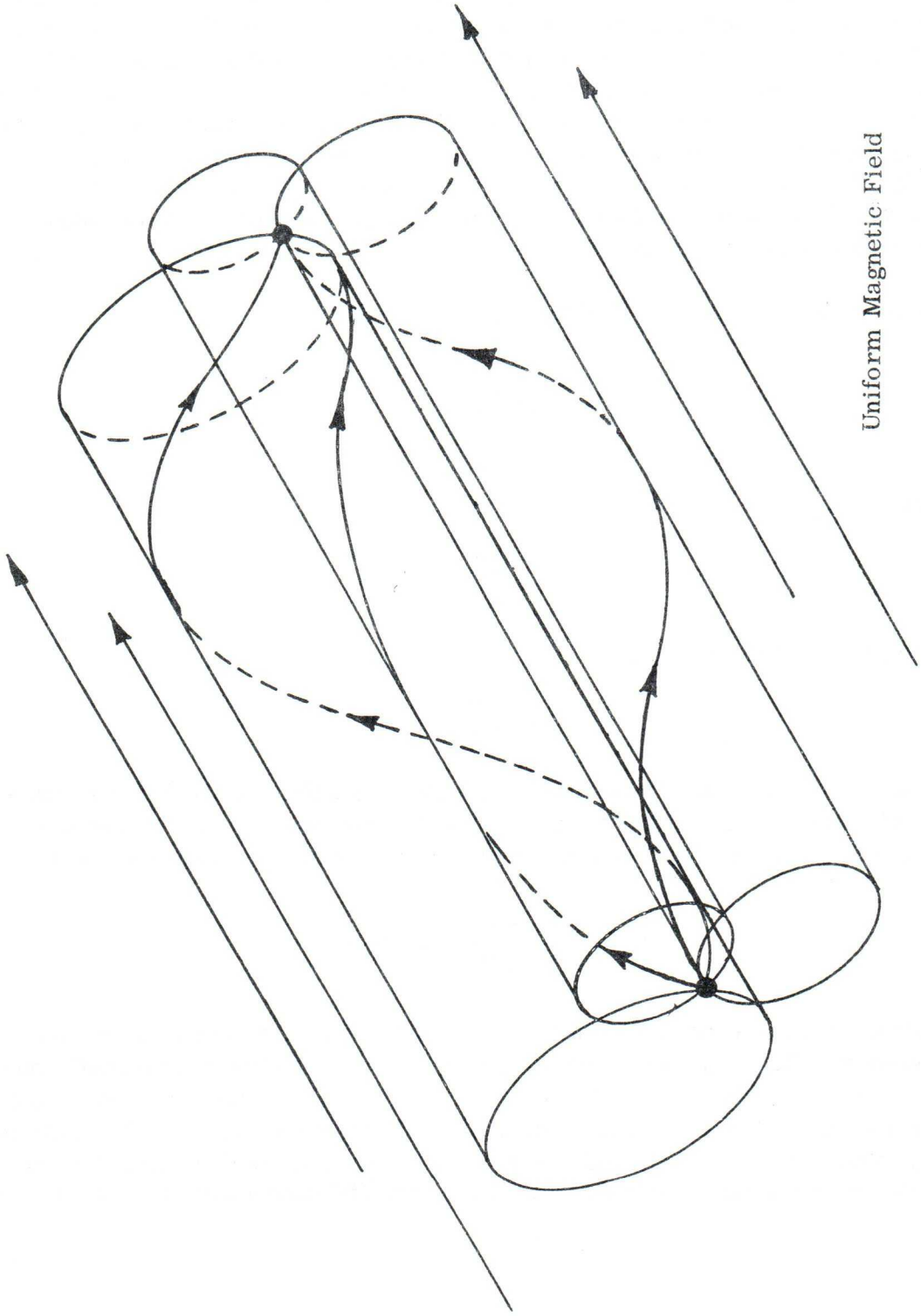

Figure 4 Helical Paths of Electrons in a Uniform Magnetic Field

upon one point P^1 of the anode. Thus, it can be seen, by changing the magnetic induction B, the diverging electron beam described can be concentrated at point P^1 of the anode by adjusting the magnetic induction B for proper focusing.

It can be described briefly, in light of the previous paragraphs, what happens when a magnetic field is introduced with an induction B_z in an axial direction and with its lines of induction running parallel to the direction of motion of the electron, while locally a uniform magnetic field with an induction B_y is introduced perpendicular to the direction of motion. The magnetic induction of this resultant field is equal to:

$$B_r = \sqrt{B_z^2 + B_y^2}$$

while the angle between B_r and B_z is given by

$$\tan y = \frac{B_y}{B_z}$$

If the velocity v is again resolved into a component $v_1 = v \cos y$ along B_r and a radial component $v_2 = v \sin y$, it is found that the latter will cause a spiral movement as before, but this time round a cylinder of which the axial direction is equal to the direction of B_r. This is so because, as already described, when an electron is moving exactly parallel to the lines of induction, it will not be subjected to any deflecting force and will be able to continue its way undisturbed at a rate of v. Hence, it can be shown that a combination of two magnetic fields, one in the axial direction of the dissector tube and the other at right angles to it, can be used to direct the photoemitted electrons from any point on a line on the cathode to the aperture of the anode. Also, a combination of three magnetic fields, one in the axial direction of the tube and the other two at right angles to it and at right angles to each other, can be used to direct the photoemitted electrons from any point on the entire cathode to the aperture of the anode. The three magnetic fields discussed can be produced by a focus coil and two sets of deflection coils as shown in Figures 1 and 2.

It has been assumed in the above discussions, for theoretical understanding only, that all the electrons are emitted from the photocathode with a velocity v and that they remain at that same velocity throughout their course until they arrive at the anode. Actually, during the operation of an image dissector tube, the electrons are emitted from the photocathode with almost a zero velocity but they are accelerated to higher velocities by means of an electric field between cathode and anode.

The following paragraph discusses the axial velocity that the accelerated electron achieves upon reaching the anode.

Assume that an electron is released from a photoemission cathode C with an initial velocity almost equal to zero (see Figure 5) and that a distance L from that surface, there is an anode A at a positive potential V with respect to C. The electron will be accelerated by the action of the field between cathode and anode. If the gradient of the potential between the plates C-A is defined by E, then

$$E = \frac{V}{L} \quad \text{(volts/meter)},$$

and the force F acting upon the electron is

$$F = eE \quad \text{(Newton's)},$$

where e is the charge of the electron in coulombs. When, as a result of that force, the electron has traveled the distance L (in meters), the amount of energy is

$$FL = eV \quad \text{(Newton - meters)}.$$

This must be equal to the kinetic energy $1/2mv^2$ which the electron has received upon reaching the anode, so that:

$$\frac{1}{2} mv^2 = eV$$

from which it follows that:

$$v = \sqrt{\frac{2eV}{m}} \quad \text{(meters/sec.)}.$$

now

$$\frac{e}{m} = 1.77 \times 10^{11} \text{ coulombs/kg},$$

so that:

$$v = 5.95 \times 10^5 \sqrt{V} \text{ (meters/sec.)};$$

or in other words: the velocity of an electron is proportional to the square root of the potential difference traversed. Further, from the above equation, it is seen that, after traversing a potential difference of 1 volt, a stationary electron obtains a velocity of 595 km/sec. This is briefly referred to as one-volt electron, and it is also said that this electron has a kinetic energy of one electron-volt. When this electron, after having been accelerated to a velocity v in the electric field between cathode and anode, emerges through an opening into a space where there is no field, it will not suffer any further changes in velocity and will continue at a uniform speed. For voltages greater than 25 kilovolts, at which the electron obtains a velocity greater than one-third the speed of light, the equation no longer applies, since the mass m of the electron was assumed to be a constant. From Einstein's theory of relativity, it follows that at high velocities the mass m increases, this increase being greater the closer the speed of light is approached. For a more thorough discussion of this, reference is made to Television by Kerkoff and Werner, pp. 21-22.

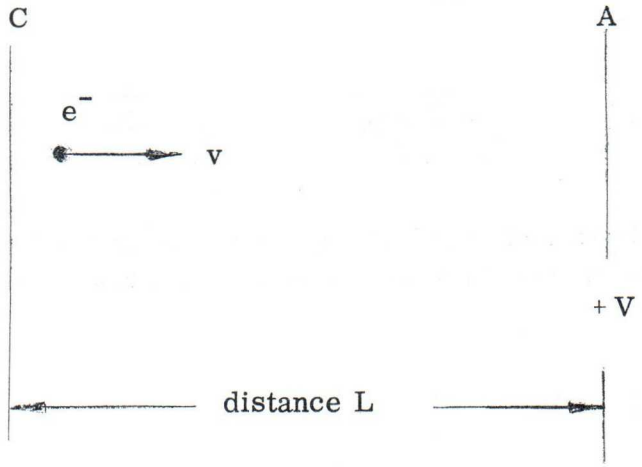

Figure 5

The following is a derivation of the relationship between the accelerating potential used and the magnetic induction required for proper focusing of electrons. The axial force on the electron is

$$F = m \frac{d^2 l}{dt^2} = E e$$

Integrating:

$$m \frac{dl}{dt} = Eet + C_1$$

Integrating again:

$$ml = \frac{Eet^2}{2} + C_1 t^{o} + C_2^{o}$$

Inserting limits of integration

$$ml \Big|_0^L = \frac{Eet^2}{2} \Big|_0^T$$

$$mL = \frac{Eet^2}{2}$$

$$T = \sqrt{\frac{2mL}{eE}} = L\sqrt{\frac{2m}{eV}} \quad \text{(sec.)}$$

Now it already has been shown that the period of a circular orbit of an electron traveling with a component of velocity at right angles to a magnetic field in which it is traveling is equal to:

$$T = \frac{2\pi m}{eB} \quad \text{(sec.)}$$

Hence, setting the time of travel of electron from cathode to anode equal to the period of a circular orbit,

$$L = \sqrt{\frac{2m}{eV}} = \frac{2\pi m}{eB}$$

$$B = \frac{\sqrt{2}\,\pi}{\left(\frac{e}{m}\right)^{1/2}} \times \frac{V^{1/2}}{L} = 0.108 \times 10^{-4} \frac{V^{1/2}}{L} \text{ webers/meter}^2$$

$$\text{or } B \approx 0.1 \times \frac{V^{1/2}}{L} \text{ gauss.}$$

where V is in volts, and L in meters. Notice from the above equation that the magnetic induction necessary for proper focusing is proportional to the square root of the accelerating potential. If L, the distance between the cathode and anode, is fixed, proper focusing may be achieved by either changing the accelerating potential V, or by changing the magnetic flux density B. But from the equation it can be seen that less change in B is required, percentagewise, than in V for proper focusing. Also, it is usually much easier to adjust the current in a focus coil than it is to vary a high voltage. Hence, this is the manner in which proper focusing is normally achieved.

Thus far in the analysis of the motion of an electron in an electric and/or a magnetic field some assumptions had to be made. In the first place we studied the motion of an electron which had a constant velocity v with a direction at some small angle to the direction of the lines of induction of a uniform magnetic field. Here the resultant motion was a helical path, the radius of which was constant as long as the velocity did not change.

Next we studied the spiral path (not truly a helical path) that an electron takes as it leaves the cathode with a low initial velocity at some angle to the lines of induction of a uniform axial magnetic field and as it is accelerated toward the anode by an axial electric field. Although the axial velocity changes, the circular velocity remains the same throughout the electron's journey from cathode to anode. A mathematical expression was derived showing the relationship between the accelerating potential and the magnetic induction required for proper focusing.

Now if a uniform magnetic field with its lines of induction running perpendicular to the axis of the dissector tube is introduced along with a uniform axial magnetic field and an accelerating potential between cathode and anode, the electron path is not as clearly defined as before. The combination of the two magnetic fields which are at right angles to each other forms a resultant magnetic field whose lines of induction run at some angle to the axis of the dissector tube. In this case, as the electrons are being accelerated toward the anodes, the velocity component perpendicular to the lines of induction of the resultant magnetic field is changing as well as the velocity component parallel to those lines. Knowing that the radius of the circular orbit is proportional to the velocity which is at right angles to the lines of induction of a magnetic field, we see that the spiral is expanding as it approaches the anode.

In order to avoid a complicated and lengthy mathematical description of the true electron path, let us suffice to say that the electron travels a path which is almost a true helix.

Experimental evidence shows that an optical image projected onto a photocathode is reproduced as an electron image at the anode with some degree of rotation. Mullard Limited has carried out some investigation of this phenomenon and has found that the amount or rotation increases as the diameter of the focus coil is made smaller. It is believed, from this evidence, that the curvature of the lines of induction of the magnetic field away from the region of the center of the focus coil cause this observed rotation to exist. A truly homogeneous magnetic field, theoretically, causes no rotation of the image.

Now that the electrons have passed through the aperture, secondary emission multiplication is used to provide amplification of the weak electron current. (See Figure 6.)

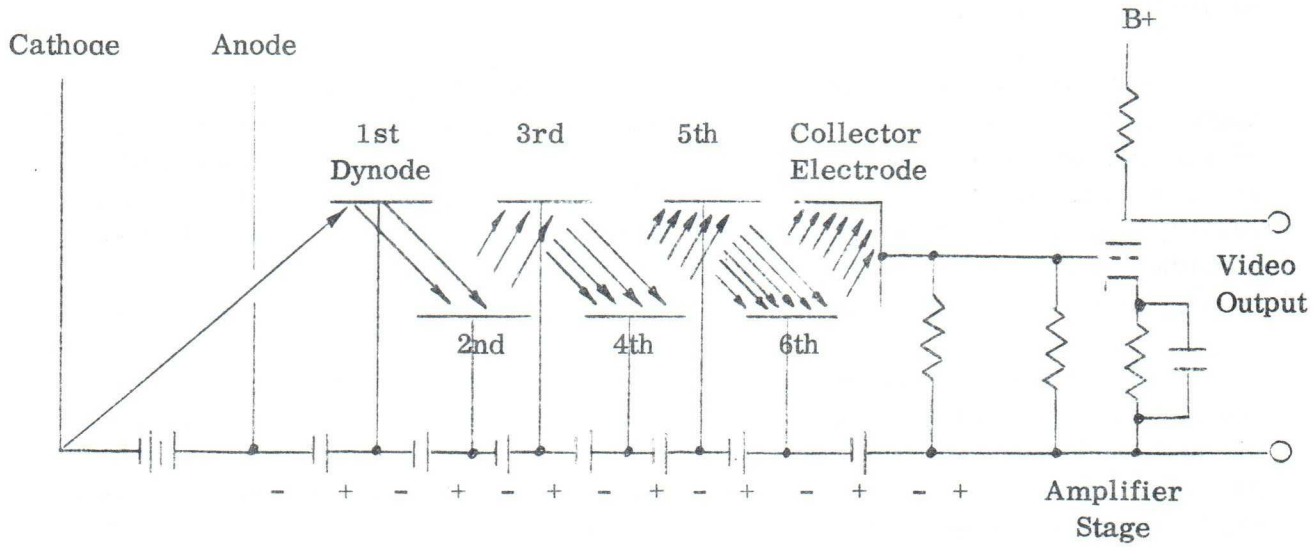

Figure 6 Secondary Emission Multiplier

This is necessary because of the relatively small number of electrons which are emitted from a photocathode that is subjected to light intensity equivalent to a bright outdoor scene. After acceleration of the electrons to a velocity at the anode equivalent to V volts (the potential between cathode and anode), and after passing through the aperture, they bombard an electrode which is called the first dynode.

Depending upon the nature of the surface bombarded and upon conditions of bombardment, a number of electrons, called secondary electrons, are re-emitted from the dynode surface. Usually the number of electrons released are greater than the number of electrons bombarding the surface by a factor of from two to five. An electric field must be provided near the dynode surface to accelerate these electrons away from the metal.

These accelerated secondary electrons now become the primary electrons which bombard the second dynode. This second dynode, in turn, re-emits more electrons. This process is continued through several stages of multiplication until the number of electrons is at least 1000 times as great as the original ones. By proper selection of operating voltages of the dynodes, a stable output current may be obtained that is proportional to the number of primary electrons originally passing through the aperture. This instantaneous output current is analog representation of the magnitude of light intensity falling upon a particular element of the photocathode surface of the image dissector.

BIBLIOGRAPHY

1. Reference Data for Radio Engineers, ITT Corporation, pp. 407-411.

2. College Physics, by Sears and Zemansky, pp. 562-565.

3. Radio Engineering, by Terman. pp. 100-103, pp. 735-738.

4. Television Engineering, by Fink, pp. 163-165.

5. Principles of Television Engineering, by Fink, pp. 126-130, pp. 134-137.

6. Television Principles, by Dome, pp. 15-16.

7. Television, by Kerkhof and Werner, pp. 20-22, pp. 25-29, pp. 41-51.

8. Television, by Zworykin and Morton, pp. 22-41, pp. 230-233.

9. Preliminary Valve Data on ME1201A, ME1201AB, ME1201AG, issued by Technical Service Department, Valve Department, Mullard Limited. (Represented by International Electronics Corporation, 137 Hudson Street, New York 13, New York.)